Title: A simple but effective model for characterizing SPR joints in steel sheet

Author: Rezwanul Haque Neal S. Williams Stuart E. Blacket Yvonne Durandet

PII: S0924-0136(15)00162-4
DOI: http://dx.doi.org/doi:10.1016/j.jmatprotec.2015.04.006
Reference: PROTEC 14376

To appear in: *Journal of Materials Processing Technology*

Received date: 9-10-2014
Revised date: 3-4-2015
Accepted date: 4-4-2015

Please cite this article as: Haque, R., Williams, N.S., Blacket, S.E., Durandet, Y.,A simple but effective model for characterizing SPR joints in steel sheet, *Journal of Materials Processing Technology* (2015), http://dx.doi.org/10.1016/j.jmatprotec.2015.04.006

A simple but effective model for characterizing SPR joints in steel sheet

Rezwanul Haque[1, #, a], Neal S. Williams[2, b], Stuart E. Blacket[2, c], Yvonne Durandet*[1, d]

[1] Swinburne University of Technology, Faculty of Science, Engineering and Technology, Industrial Research Institute Swinburne (IRIS), Hawthorn, VIC 3122, Australia

[2] Henrob (UK) Pty Ltd, Geebung, Brisbane, QLD 4034, Australia

[a]rhaque@usc.edu.au, [b]nsw@henrob.com.au, [c]SEB@henrob.com.au, [d]ydurandet@swin.edu.au

*Corresponding author. Tel.: +61 3 9214 5720; Fax: +61 3 9214 8264.
Email address: ydurandet@swin.edu.au (Y. Durandet)
Postal address: Swinburne University of Technology, Faculty of Science, Engineering and Technology, P.O. Box 218, Hawthorn, Victoria 3122, Australia

[#] Now at the University of the Sunshine Coast, Faculty of Science, Health, Education and Engineering, School of Science and Engineering, Sippy Downs, QLD 4556, Australia

Abstract

A simple and effective model has been developed to determine rivet flaring in self-piercing riveted (SPR) joints. Both interrupted and un-interrupted SPR experiments were performed with recording of force and punch displacement data. Based on the analysis of experimental SPR process data and the examination of cross-sections of SPR samples, two key points of the force-displacement curves were identified that mark the start (d_0) and end (d_{max}) of rivet flaring respectively. It was found that these two events were able to be related to the path of the tip of the flaring rivet and hence the internal characteristics of the SPR samples via a simplified geometric approach. A linear relationship between the rivet flaring and (d_{max}-d_0) was thus established. The study shows that in the absence of a finite element model, the experimental characteristic force-displacement curve can be used directly to estimate the rivet flaring without having to cut the SPR joint.

Keywords: self-piercing riveting, joint quality, rivet flaring model, characteristic force-displacement curve, joining by forming, SPR

1. Introduction

Self-piercing riveting (SPR) is a mechanical fastening technique used for spot joining of sheet materials. This technique is increasingly adopted by the automotive industry because of the growing use of light weight or dissimilar metals that are difficult to spot weld such as galvanized steel, aluminium and magnesium alloys. As shown in Fig. 1, to produce an SPR joint, a tubular rivet is driven through the top sheet,

piercing (not perforating) the bottom sheet and flaring in the bottom sheet under the guidance of a suitable die that is positioned underneath. The flaring of the rivet in the bottom sheet produces the mechanical interlock between the sheets. Hence, a good joint should have sufficient but not excessive flaring of the rivet in the bottom sheet as the joint strength directly depends on the amount of rivet flaring.

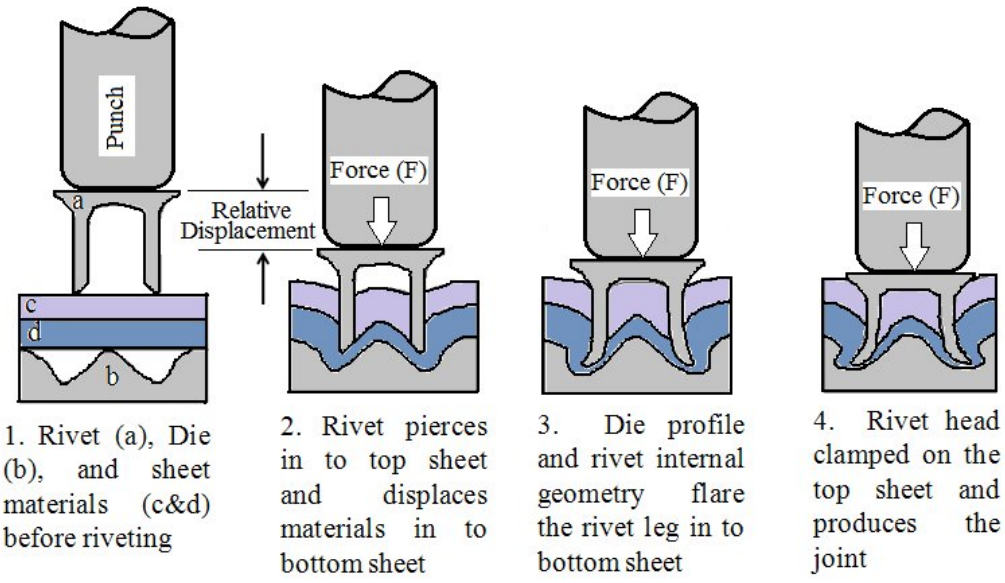

Fig. 1 Schematic diagram of self-pierce riveting (SPR) process adopted from Haque et al. (2012b)

SPR is a complex and intricate process of joining by forming. Meschut et al. (2014) reported that nowadays, ultra-high strength materials and alloys are used in automotive industries, where limited deformation under load is required. Thus, it is necessary to understand the deformation behaviour of sheet material and rivet during the SPR process. Finite Element Analysis (FEA) is a useful tool to gain more

understanding and optimize the process in order to join new alloys and materials, and finally to predict the mechanical behaviour of the SPR joint.

For example, to study the mechanism of joint formation (filling of the die and rivet bore and rivet flaring), Atzeni et al. (2009) created a 2D finite element model using ABAQUS. They validated their model by comparing the predictions of force-displacement curve and cross-section of a joint with experimental data for 2-stack SPR joints (3 mm + 3 mm AA 6082-T4).

Casalino et al. (2008) reported good agreement between their simulated and experimental results (force-displacement curve and cross-sectional geometry) for SPR joining of thin aluminium alloy (1.8 mm + 1 mm AA 6060 T4) with software LS-DYNA. They found that the results were highly dependent on the mesh size, proper assumption of plastic strain and associated failure criterion (kill-element technique).

Abe et al. (2006) conducted a join-ability study for high strength steel with aluminium by LS-DYNA. They found that their model outputs were consistent with the experimental force-displacement curves and joints' cross-sections when the value of the friction coefficient between all interfaces was assumed to be 0.2. Moreover to shorten the calculation time they set the punch velocity to 25 times the actual riveting speed.

Hoang et al. (2010) examined the possibility of replacing steel rivet with aluminium rivet by numerical simulation (LS-DYNA). They used the experimental force-displacement curve to validate their model and finally they characterized the mechanical behaviour by using the numerical model. However, another study by (the same authors) Hoang et al. (2013) showed that the numerical results highly depended on the proper assumption of friction coefficient.

Bouchard et al. (2008) developed a FEM model using the software package FORGE to understand the SPR process as well as to estimate joints strength in different loading conditions (cross-tension and lap shear). They concluded that it is necessary to include the material history (damage that occurred in rivet and sheet material during riveting) for better prediction of the joint strength. They also validated their model of the SPR process against the experimental force-displacement curve. Grujicic et al. (2014) also proposed a computational approach to establish the effect of process and materials parameters on the quality and mechanical performance of the SPR joint. They found that FEM approach could be a useful tool to adjust the SPR process and material selection in order to obtain a desired joint performance.

Mucha (2011) performed a numerical simulation to optimize the industrial productivity of the riveting process. He found that proper selection of the die significantly influences the finished joint. Mucha (2013) also studied the effect of material properties and other process parameters on joints made with solid rivets. He showed that various joint strengths may be achieved by controlling the joint forming force. Thus it is also important to monitor the joint forming force.

Markowski et al. (2013) completed a numerical simulation to study the effect of joint forming force on clinched joint by taking into account the rigidity of the machine's C-frame. They showed that the design of the C-frame has a significant impact on the joint forming force as the tool positioning depends on the amount of C-frame deflection.

He et al. (2013a) developed a quality monitoring system of the SPR joints by numerical simulation. They validated their model by comparing the experimental force-displacement curve with the numerically obtained force-displacement curve.

The same group of authors He et al. (2013b) extended their investigation to evaluate the joint strength and energy absorption for bonded SPR joints. Similar validation techniques were followed and good agreement was found between the numerical and experimental results. Han et al. (2014) developed a numerical model to predict the joint quality depending on the die design parameters. They concluded that their simulation was useful for designing the die parameters.

Hence, most FEA studies reported in the literature as cited by Groche et al. (2014) make use of experimental force-displacement curves and joint cross-sections to validate the finite element models. The force-displacement curve can also be used as a tool to monitor the SPR process, as shown by King (1997). However, very few studies have been published on actual SPR force-displacement data curves and how to directly extract more information from them in order to characterize the riveting process.

The present study was undertaken to examine whether the amount of rivet flaring can be determined directly from SPR process data (force-displacement curve). A relationship between the characteristic experimental force-displacement curve and the rivet flaring is proposed in this paper.

2. Experimental Procedure

In order to develop a model which can predict the rivet flaring inside a joint, six different complete joints were produced using steel sheets (yield strength 300 MPa and hardness 198 HV, in Australia known as G300 steel) with three different thicknesses and steel rivets with three different hardness levels (Table 1). More details

on the steel properties can be found in Bluescope (2015). These joints were also interrupted at different positions using the method provided in Haque et al. (2012a). The length of the rivet was chosen according to the total ply thickness, and the die was chosen accordingly.

Table 1: Joining parameters (all materials are the same grade of carbon steel, pre-clamp and rivet setting pressure were 125 and 220 bar, respectively)

Condition		**1**	**2**	**3**	**4**	**5**	**6**
Thicknesses of ply materials (mm)		2.5 + 2.5	2 + 2	2 + 2	2 + 2	1.5 + 1.5	1.5 + 1.5
Rivet	Length (mm)	8	7	7	7	6	6
	Hardness (HV)	555	555	480	410	480	410
Die (flat die profile)	Depth (mm)	3	2.5	2.5	2.5	2.3	2.3
	Diameter (mm)	10	10	10	10	9	9
Coefficient depends on rivet hardness (C1).		0.43	0.43	0.55	0.66	0.55	0.66
Coefficient depends on rivet length (C2).		0.90	0.67	0.67	0.67	0.60	0.60

SPR trials were conducted using Henrob's 2-stage hydraulic rivet setter with pre-clamp. Sheet coupons were setup on a fixture table to make the joints. A load cell, a linear variable differential transformer (LVDT) and pressure transducers were used to measure the force, punch displacement, rivet setting and pre-clamp pressure respectively as a function of time. The experimental setup and method of producing the characteristic force-displacement curve taking into account the elastic deformation of the C-frame are described in detail in Haque et al. (2012a). Rivet flaring was

measured for both completed and interrupted joints from the micrographic cross-section by using a microscope (a schematic of rivet flaring is shown in Fig. 2). For each sample the measurement was conducted five times.

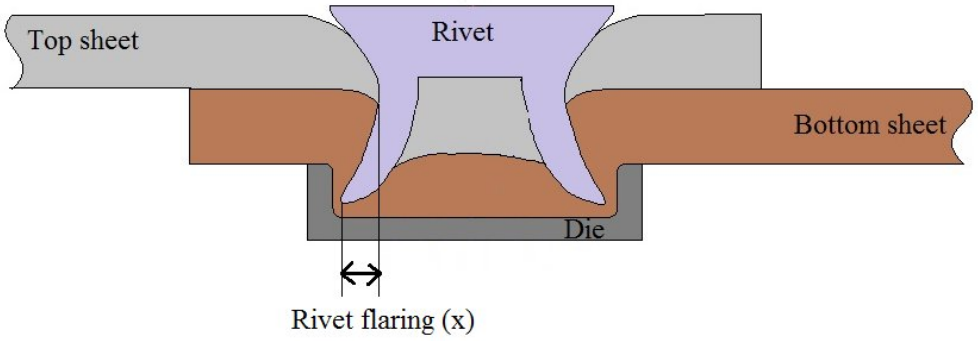

Fig. 2 Schematic of a riveted joint showing the amount of rivet flaring

3. Experimental Results

The cross-sections and related characteristic curves of the six different joint conditions are shown in Fig. 3. It was observed that for all conditions, regardless of ply material thickness and rivet length, a sharp and distinctive rise in force occurred in the characteristic curve at a force of 30 kN.

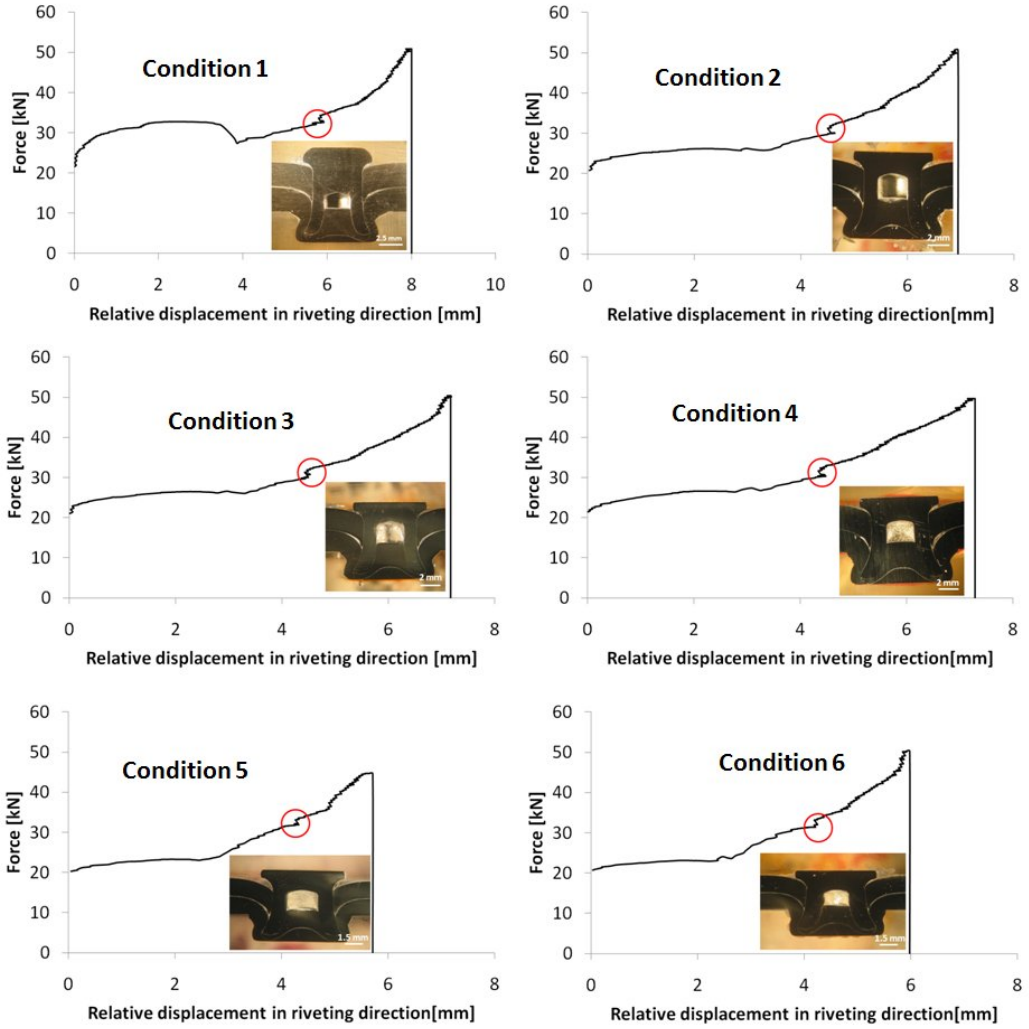

Fig. 3 Step rise of force for six different conditions (listed in Table 1); the photograph in each graph is a cross-section of the completed SPR joint

During the first stage, bending of sheet material occurred and the die was filled partially by the material. Plastic deformation occurred, but there was no shearing as the ultimate strength of the material was above the stress produced during this period. As soon as the force reached the ultimate strength of the material, ductile shearing initiated in the top sheet, i.e. piercing started, which is characterized as the second stage. Again when the bottom sheet touched the die floor, material movement in the

riveting direction was no longer possible towards the die, i.e. vertically. The rivet then started to flare because of the reaction force of the die. From the characteristic curve, the displacement of rivet before flaring (d_0) and maximum rivet displacement (d_{max}) can be obtained, as shown in Fig. 4.

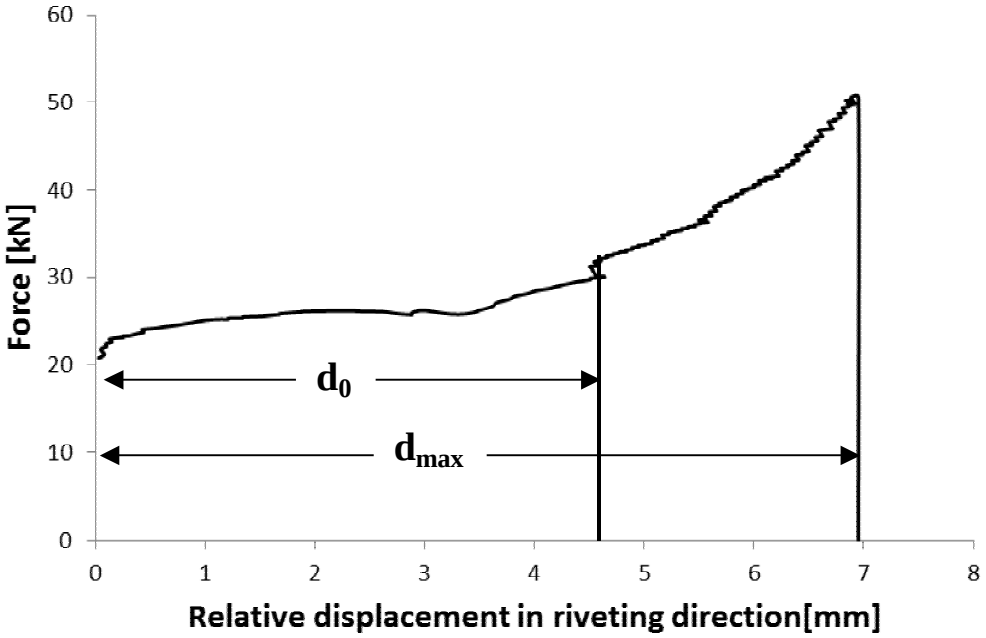

Fig. 4 Characteristic-curve of 2 mm + 2 mm carbon steel joint with a 7 mm long rivet having a hardness of 555 HV

It is proposed that the shank of the rivet remains straight up to the distance of d_0 as the horizontal component of the reaction force (F_H in Fig. 5) is not enough to deform the rivet material. As soon as the horizontal force vector F_H exceeds the resistance of the rivet wall, the rivet starts flaring. To test the above hypothesis, the joints were interrupted at several punch positions on either side of this critical point. Examples of

such tests are shown in Figs. 6a-c. It was found that for all joining conditions, the rivet started to flare after a certain value of force was reached.

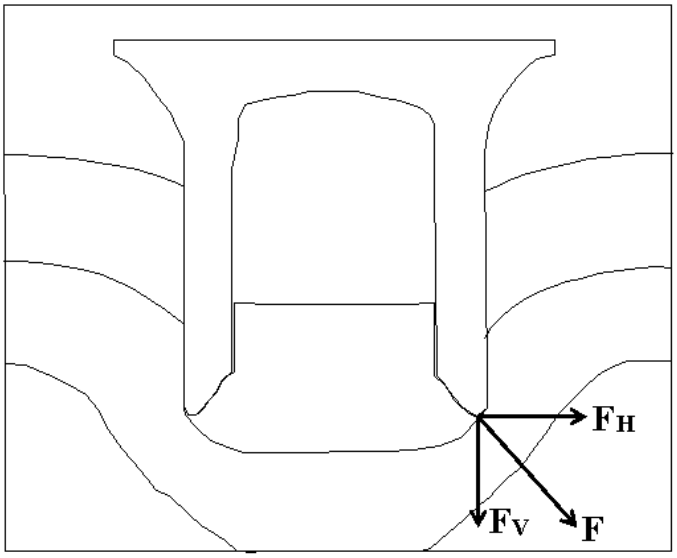

Fig. 5 Schematic diagram shows the starting point of rivet flaring

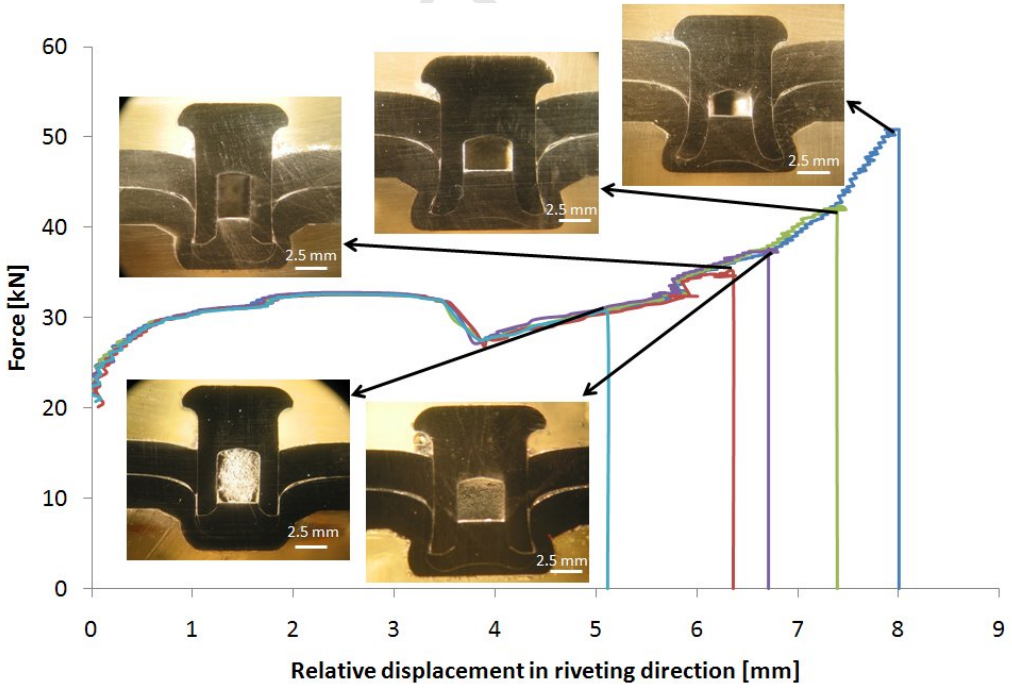

(a)

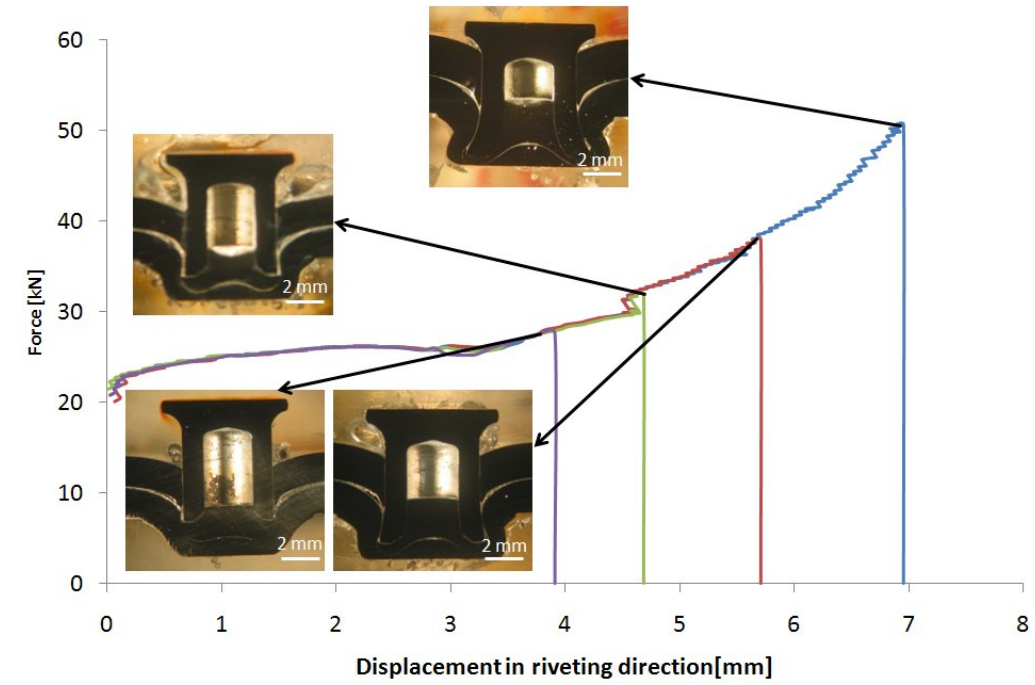

(b)

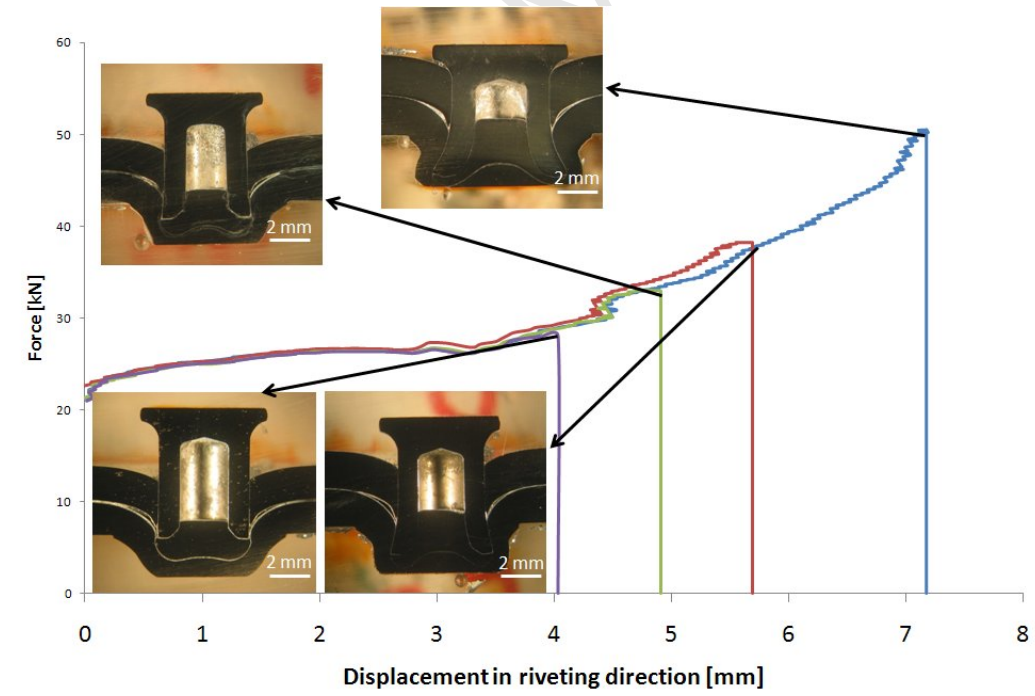

(c)

Fig. 6 Interrupted SPR process for conditions (a) 1, (b) 2 and (c) 3 in Table 1; the photographs are cross-sections of interrupted joints

Once the start of rivet flaring has been identified, it is necessary to find the path of the rivet tip. For this, the joints were interrupted at different positions before the complete joints and the amount of flaring was measured for each interrupted position. Results show a linear dependence of the measured rivet flaring upon the interrupted punch position (Fig. 7). This observation was used to develop the rivet flaring model presented in the next section.

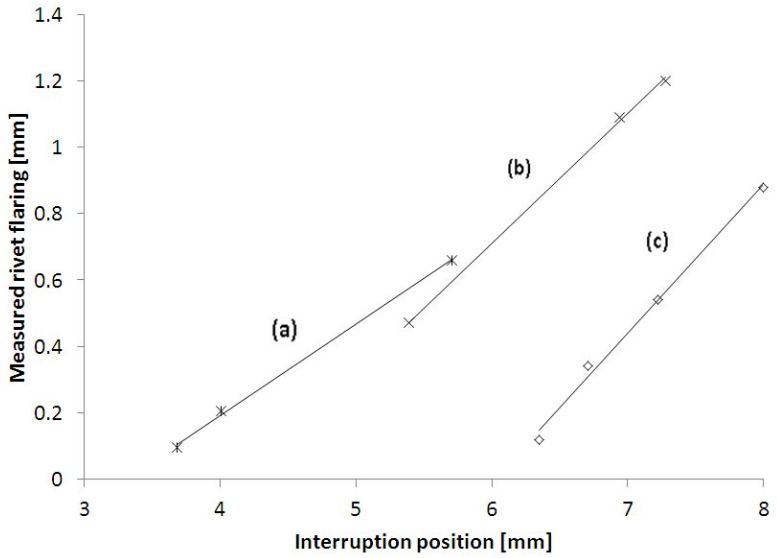

Fig. 7 Rivet flaring dependence on interrupted position for different stacks of carbon steel sheet thicknesses: (a) condition 5: 1.5 +1.5 mm joint, (b) condition 4: 2 +2 mm joint, and (c) condition 1: 2.5 +2.5 mm joint

4. Proposed rivet flaring model

It is assumed that the rivet travels a distance d_0 in the vertical direction before it starts to flare, and that flaring starts because of the reaction force from the die. The concept for the rivet flaring model is shown schematically in Fig. 8. Flaring starts in the OE direction because of the die reaction. The joint is completed when the rivet tip reaches point C on line OE.

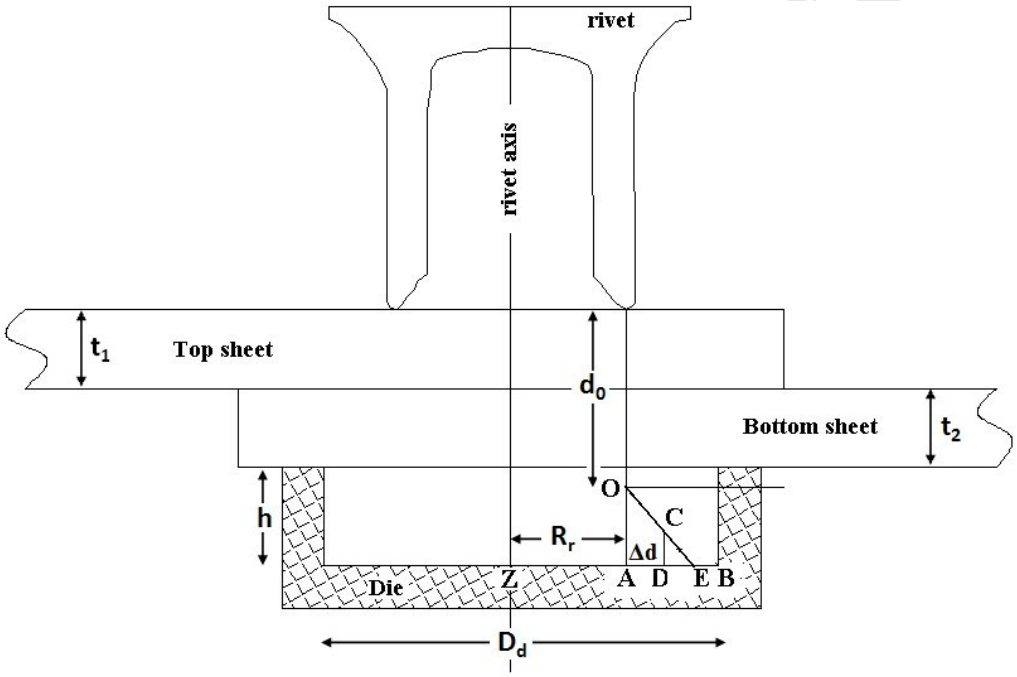

Fig. 8 Geometrical model of rivet flaring calculation, where Δd (distance AD) is the rivet flaring

It is difficult to find the point E on AB because rivet flaring depends on the hardness of the rivet, which determines the angle AOE. In the proposed model, point E on AB is approximated by equation 1:

$$AE = C_1 * AB = C_1 * (ZB - ZA) = C_1 * (D_d/2 - R_r) \quad (1)$$

where C_1 is a coefficient that depends on the rivet hardness, ZB is the die radius ($D_d/2$) and ZA is the rivet shank radius before flaring (R_r).

When the rivet is very hard compared with the sheet material, little or no flaring of the rivet will occur and the rivet tip will move from point O towards point A and point E will coincide with point A. Thus the length AE will reach maximum when E coincides with B, and in that case AE equals AB. So the range of the coefficient for rivet hardness is: $0 \leq C_1 \leq 1$. For a given stack of material, increasing the rivet hardness delays the start of flaring, resulting in larger d_0 value on the force displacement curve, and reduced rivet flaring or interlock, as discussed previously in Haque et al. (2012a).

Points O, A and E on the triangle OAE can be found from the following geometric relationships:

$$OA = (t_1 + t_2 + h - d_0) \tag{2}$$

$$OE = \sqrt{OA^2 + AE^2} = \sqrt{(t_1 + t_2 + h - d_0)^2 + (C_1 * (\frac{D_d}{2} - R_r))^2} \tag{3}$$

Where t_1 and t_2 are top and bottom sheet thickness respectively and h is die depth.

For the path of the rivet tip, it has been assumed that OE is a straight line. Hence,

$$OC = C_2 * (d_{max} - d_0) \tag{4}$$

where C_2 is a coefficient that depends on rivet length. C_2, like C_1, also ranges from 0 to 1 according to whether the rivet flares not at all or fully.

It is now possible to calculate the rivet flaring (Δd) from a simple geometrical relation:

$$\Delta d = AD = \frac{OC * AE}{OE} \tag{5}$$

Substituting values of AE, OE and OC from equations 1, 3 and 4 respectively, equation 5 can be rewritten in the following form.

$$\Delta d = \frac{C_2*(d_{max}-d_0)*C_1*(\frac{D_d}{2}-R_r)}{\sqrt{(t_1+t_2+h-d_0)^2+(C_1*(\frac{D_d}{2}-R_r))^2}} \quad (6)$$

For a given die and rivet, the die diameter (D_d), die depth (h) and rivet radius (R_r) are known. For a given joint, the top sheet thickness (t_1) and bottom sheet thickness (t_2) are also known, and d_{max} and d_o can be obtained from the characteristic force-displacement curve.

Based on the assumption of a linear flaring trajectory along OE (Fig. 8), the coefficients C_1 and C_2 in equation (6) were thus determined empirically for the different joint conditions 1 to 4 (Table 1) (using the interrupted test results. It was found that C_1 decreased with rivet hardness as expected from equation (1), whereas C_2 increased with rivet length as inferred from equation (4). The coefficients values ranged from 0.4 to 0.7 for C_1 and from 0.6 to 0.9 for C_2.

After determining the coefficients C_1 and C_2 from the interrupted samples, equation (6) was then used to calculate the rivet flaring for the complete joints for conditions 1-4 and 5-6.

It was found that the calculated rivet flaring using equation (6) was in good agreement with the measured rivet flaring for all completed joints. As shown in Fig. 9, the calculated rivet flaring was plotted against the measured rivet flaring, and the displayed 45° line highlighted the good fit for all conditions. A comparison of the studied variable is also shown in Fig. 10 in the form of a bar chart.

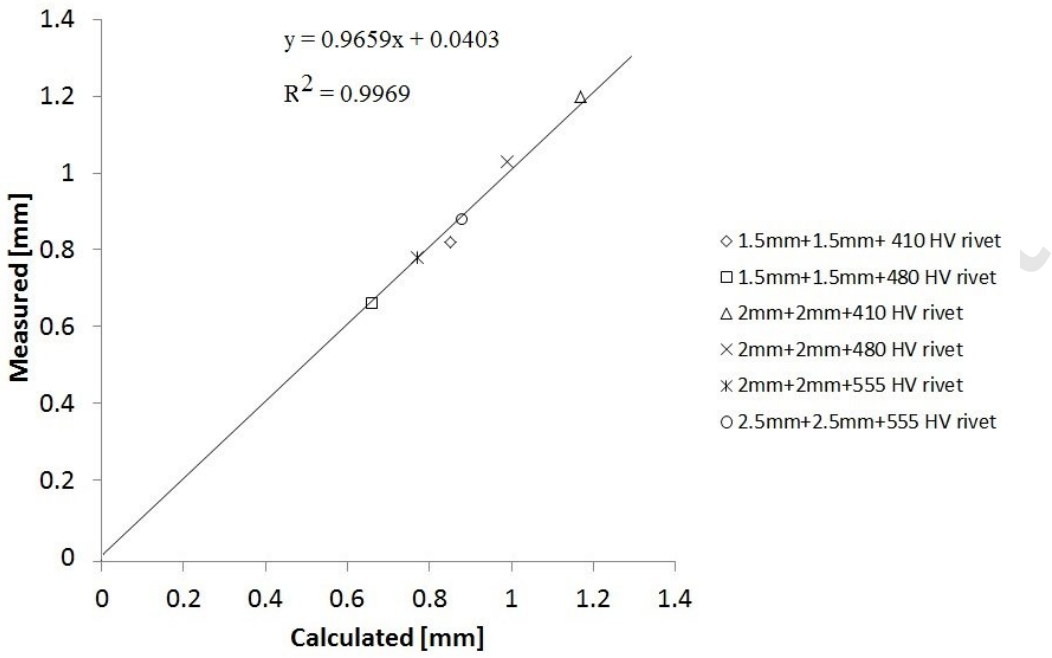

Fig. 9 Rivet flaring calculated vs. measured for the six different full joint conditions in Table 1

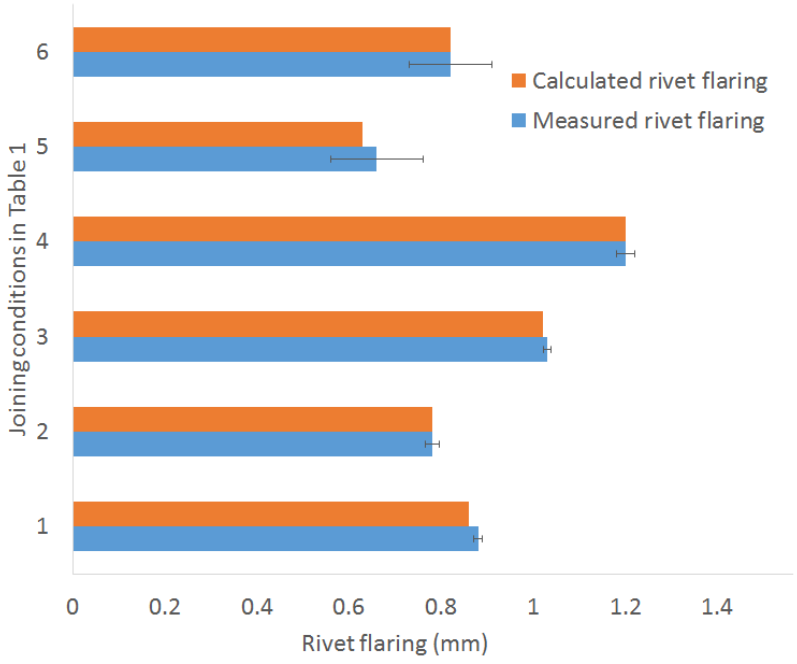

Fig. 10 Comparison of calculated and measured rivet flaring values for the six different full joint conditions listed in Table 1

Hence, this simple formula can successfully be used to estimate the rivet flaring without having to cross-section a joint. The coefficients used in this formula are dependent only on rivet properties (hardness and length), whereas d_o and d_{max} which are given by the characteristic process curve, account for the properties of the ply materials. It should be noted that C_1 coefficients were determined for a range of rivet hardness from 410 HV to 555 HV, and C_2 coefficients were for a range of rivet length from 6 mm to 8 mm, which represent the range of data used to generate the formula for the conditions examined in the present study.

After successful prediction of rivet flaring for the above six conditions, equation (6) was also used to predict the rivet flaring for other completed joints. Six additional joints were produced using different sheet thickness and hardness, die depth and rivet setting pressure as listed in Table 2. It was found that the rivet flaring calculated using equation (6) was in good agreement with the measured rivet flaring for all completed joints, as shown in Fig. 11. This confirmed that the validity of the proposed model.

Table 2: Joining parameters (Materials are of different grades, 125 bar pre-clamp and 250 bar rivet setting pressures)

Condition		**7**	**8**	**9**	**10**	**11**	**12**
Hardness of ply materials (HV)		270	192	270	192	270	192
Thicknesses of ply materials (mm)		2.5 + 2.5	2.5 + 2.5	2 + 2	2 + 2	1.5 + 1.5	1.5 + 1.5
Rivet	Length (mm)	8	8	7	7	6	6
	Hardness (HV)	555	555	480	480	480	480
Die (flat die profile)	Depth (mm)	2.35	2.35	2.1	2.1	2.0	2.0
	Diameter (mm)	11	11	10	10	9	9
Coefficient depends on rivet hardness (C1).		0.43	0.43	0.66	0.66	0.66	0.66
Coefficient depends on rivet length (C2).		0.90	0.90	0.67	0.67	0.60	0.60

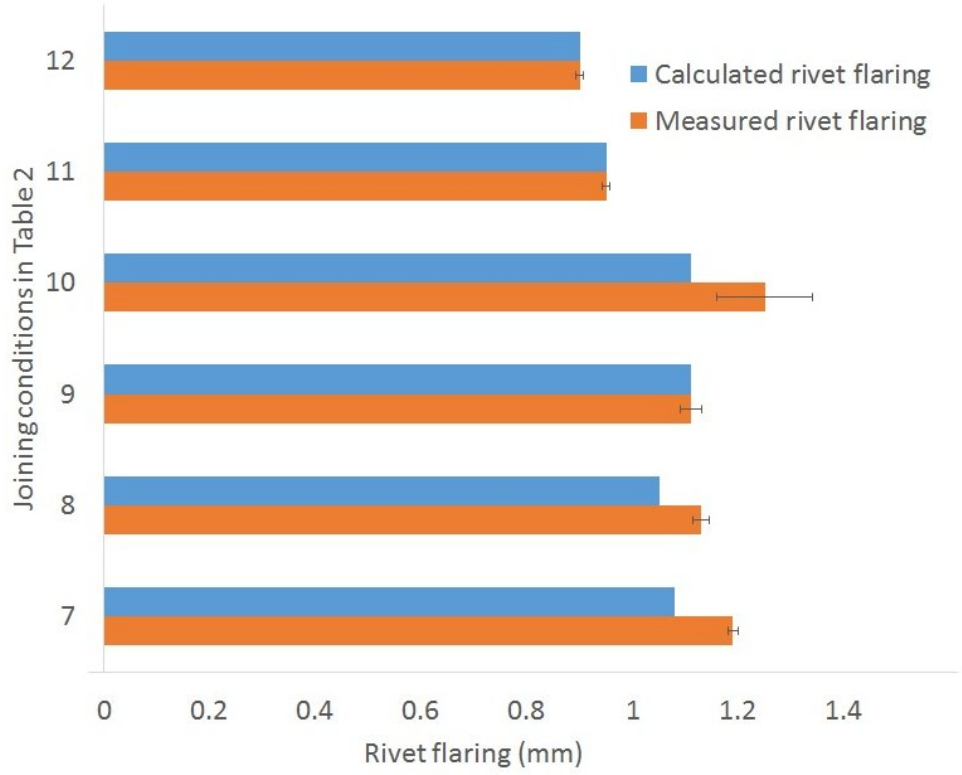

Fig. 11 Comparison of calculated and measured rivet flaring values for the additional six different full joint conditions listed in Table 2

Equation (6) could be improved by considering the path of the rivet tip OE as a parabola rather than a straight line. Considering the simple nature of this equation, reasonably good agreement was achieved between the calculated and measured rivet flaring for interrupted cases. From an industrial viewpoint, interrupted joints are not of interest. Equation (6) gives very good results to determine rivet flaring for a completed joint.

The rivet flaring calculator can be used to improve and optimize an SPR joint for a given material and thickness combination. In practice, it is very easy to pick up the displacement (d_{max}-d_0) and for an operator to decide whether the joint is good or bad in terms of rivet flaring. However, the quality of an SPR joint does not depend solely on rivet flaring; it depends on other factors such as: flaring angle, effective contact length between rivet and tail side material. Some of the factors could be found from the characteristic force-displacement curve.

5. Conclusions

This paper presents a simple geometrical method to calculate rivet flaring without having to cross-section a joint. It is a non-destructive testing method of determining rivet flaring based on the characteristic force-displacement curve. A relationship was established between ply thickness, nominal die and rivet dimensions, and two key

data points from the characteristic force-displacement curve. These key data points were the relative punch displacements at the start and end of rivet flaring. A linear relationship (Equation 6) was established that works within a range of steel thicknesses and comprised two coefficients which were determined empirically as functions of rivet hardness and length.

Since rivet flaring is a measure of the mechanical interlock, it is a dominant factor in determining the strength of an SPR joint, and hence the rivet flaring estimator developed in this study could be a very useful tool in joint product development and process optimization.

Acknowledgements

The support of CAST CRC and provision of a PhD scholarship are acknowledged. CAST was established under, and supported in part by the Australian Government's Co-operative Research Centre Program. The valuable feedback from Professor John Beynon to the initial drafting of this manuscript is gratefully acknowledged.

Nomenclature

C_1 = Coefficient depends on rivet hardness ($0 \leq C_1 \leq 1$).

C_2 = Coefficient depends on rivet length ($0 \leq C_2 \leq 1$).

d_0 = Displacement of rivet before flaring (mm).

D_d = Die diameter (mm).

ZB = Die radius

d_{max} = Maximum rivet displacement (mm).

h = Die depth (mm).

R_r = Rivet radius (mm).

t_1 = Top sheet thickness (mm)

t_2 = Bottom sheet thickness (mm)

Δd = Rivet flaring (mm)

References

Abe, Y., Kato, T., Mori, K., 2006. Joinability of aluminium alloy and mild steel sheets by self piercing rivet. Journal of Materials Processing Technology 177, 417–421.

Atzeni, E., Ippolito, R., Settineri, L., 2009. Experimental and numerical appraisal of self-piercing riveting. CIRP Annals - Manufacturing Technology 58, 17-20.

Bluescope (2015): http://steelproducts.bluescopesteel.com.au/home/steel-products/metallic-coated-steel, accessed on 26th January, 2015.

Bouchard, P.O., Laurenta, T., Tollier, L., 2008. Numerical modeling of self-pierce riveting—From riveting process modeling down to structural analysis. Journal of Materials Processing Technology 202, 290-300.

Casalino, G., Rotondo, A., Ludovico, A., 2008. On the numerical modelling of the multiphysics self piercing riveting process based on the finite element technique. Advances in Engineering Software 39, 787-795.

Groche, P., Wohletz, S., Brenneis, M., Pabst, C., Resch, F., 2014. Joining by forming—A review on joint mechanisms, applications and future trends. Journal of Materials Processing Technology 214(10), 1972-1994.

Grujicic, M., Snipes, J., Ramaswami, S., Abu-Farha, F., 2014. Process modeling, joint-property characterization and construction of joint connectors for mechanical fastening by self-piercing riveting. Multidiscipline Modeling in Materials and Structures 10(4), 631-658.

Han, S.-L., Li, Z.-Y., Gao, Y., Zeng, Q.-L., 2014. Numerical study on die design parameters of self-pierce riveting process based on orthogonal test. Journal of Shanghai Jiaotong University (Science) 19 (3), 308-312.

Haque, R., Beynon, J.H., Durandet, Y., 2012a. Characterisation of force-displacement curve in self-pierce riveting. Science and Technology of Welding and joining 17, 476-488.

Haque, R., Beynon, J.H., Durandet, Y., Kirstein, O., Blacket, S., 2012b. Feasibility of measuring residual stress profile in different self-pierce riveted joints. Science & Technology of Welding & Joining 17, 60-68.

He, X., Hu, Y., Xing, B., Ding, Y., Zeng K., 2013a. Numerical Simulation and Online Window Monitoring of SPR Process. Advanced Materials Research 602-604, 1765-1768.

He, X., Xing, B., Zeng, K., Gu, F., Ball, A., 2013b. Numerical and experimental investigations of self-piercing riveting. The International Journal of Advanced Manufacturing Technology 69, 715-721.

Hoang, N.H., Hopperstad, O.S., Langseth, M., Westermann, I., 2013. Failure of aluminium self-piercing rivets: An experimental and numerical study. Materials and Design 49, 323-335.

Hoang, N.H., Porcaro, R., Langseth, M., Hanssen, A.G., 2010. Self-piercing riveting connections using aluminium rivets. International Journal of Solids and Structures 47, 427–439.

King, R.P., 1997. Analysis and quality monitoring of a self-pierce riveting process, PhD Thesis University of Hertfordshire, Hertfordshire, UK.

Markowski, T., Mucha, J., Witkowski, W., 2013. FEM analysis of clinching joint machine's C-frame rigidity. Eksploatacja i Niezawodnosc - Maintenance and Reliability 15 (1), 51-57.

Meschut, G., Janzen, V., Olfermann, T., 2014. Innovative and highly productive joining technologies for multi-material lightweight car body structures. Journal of Materials Engineering and Performance 23 (5), 1515-1523

Mucha, J., 2011. A study of quality Parameters and behaviour of self-piercing riveted aluminium sheets with different joining conditions. Strojniski vestnik- Journal of Mechanical Engineering 57 (4), 323-333.

Mucha, J., 2013. The effect of material properties and joining process parameters on behaviour of self-pierce riveting joints made with solid rivet. Materials & Design 52, 932-946.

Figure and Table Captions

Fig. 1 Schematic diagram of self-pierce riveting (SPR) process adopted from Haque et al. (2012b)

Fig. 2 Schematic of a riveted joint showing the amount of rivet flaring

Fig. 3 Step rise of force for six different conditions (listed in Table 1); the photograph in each graph is a cross-section of the completed SPR joint

Fig. 4 Characteristic-curve of 2 mm +2 mm carbon steel joint with a 7 mm long rivet having a hardness of 555 HV

Fig. 5 Schematic diagram shows the starting point of rivet flaring

Fig. 6 Interrupted SPR process for conditions (a) 1, (b) 2 and (c) 3 in Table 1; the photographs are cross-sections of interrupted joints

Fig. 7 Rivet flaring dependence on interruption position for different carbon steel sheet thicknesses: (a) condition 5: 1.5 +1.5 mm joint, (b) condition 4: 2 +2 mm joint, and (c) condition 1: 2.5 +2.5 mm joint

Fig. 8 Geometrical model of rivet flaring calculation, where Δd (distance AD) is the rivet flaring

Fig. 9 Rivet flaring calculated vs. measured for the six different full joint conditions in Table 1

Fig. 10 Comparison of calculated and measured rivet flaring values for the six different full joint conditions listed in Table 1

Fig. 11 Comparison of calculated and measured rivet flaring values for the additional six different full joint conditions listed in Table 2

Table 1: Joining parameters (all materials are the same grade of carbon steel, pre-clamp and rivet setting pressure were 125 and 220 bar, respectively)

Table 2: Joining parameters (Materials are of different grades, 125 bar pre-clamp and 250 bar rivet setting pressures)